Quantum interference of tunnel trajectories between states of different spin length in a dimeric molecular nanomagnet

CHRISTOPHER M. RAMSEY[1], ENRIQUE DEL BARCO[1]*, STEPHEN HILL[2], SONALI J. SHAH[3], CHRISTOPHER C. BEEDLE[3] AND DAVID N. HENDRICKSON[3]

[1]Department of Physics, University of Central Florida, Orlando, Florida 32765, USA
[2]Department of Physics, University of Florida, Gainesville, Florida 32611, USA
[3]Department of Chemistry and Biochemistry, University of California at San Diego, La Jolla, California 92093, USA
*e-mail: delbarco@physics.ucf.edu

Published online: 2 March 2008; doi:10.1038/nphys886

Tunable electron spins in solid media are among the most promising candidates for qubits[1]. In this context, molecular nanomagnets have been proposed as hardware for quantum computation[2]. The flexibility in their synthesis represents a distinct advantage over other spin systems, enabling the systematic production of samples with desirable properties, for example, with a view to implementing quantum logic gates[3,4]. Here, we report the observation of quantum interference associated with tunnelling trajectories between states of different total spin length in a dimeric molecular nanomagnet. We argue that the interference is a consequence of the unique characteristics of a molecular Mn_{12} wheel, which behaves as a molecular dimer with weak ferromagnetic exchange coupling: each half of the molecule acts as a single-molecule magnet, whereas the weak coupling between the two halves gives rise to an extra internal spin degree of freedom within the molecule—that is, its total spin may fluctuate. More importantly, the observation of quantum interference provides clear evidence for quantum-mechanical superpositions involving entangled states shared between both halves of the wheel.

Molecular nanomagnets have become prototype systems to probe the realm that borders quantum and classical physics, as well as to study decoherence phenomena in quantum systems[4–11]. In particular, single-molecule magnets (SMMs) stand out as a magnificent example of the possibilities offered by supramolecular chemistry for the engineering of quantum properties in nanoscale systems. SMMs contain multiple transition-metal ions bridged by organic ligands. These ions are coupled by exchange interactions, often in a ferrimagnetic manner, yielding a large magnetic moment (spin) per molecule. This large spin, combined with significant uniaxial anisotropy, provides a barrier to magnetization reversal. Particularly important is the appearance of quantum tunnelling through this barrier between states with opposite spin projection, leading to step-wise magnetic hysteresis loops due to the accelerated magnetic relaxation at fields that 'switch on' the quantum tunnelling of the magnetization[12,13] (QTM). This unique feature is a consequence of the quantum superposition of high-spin states of the molecule and has resulted in the observation of a variety of fundamental phenomena[3,14–17].

Here, we investigate a new Mn_{12}-based wheel that can be modelled as two ferromagnetically coupled $S = 7/2$ SMM units giving rise to a total $S = 7$ ground state, as illustrated in Fig. 1a (see the Methods section). The magnetization curves in Fig. 1c show the characteristic steps associated with resonant QTM. Above 0.9 K, the hysteresis disappears and the data follow a Langevin function with S (= 6.97) as the only fitting parameter (dashed black line in Fig. 1c). From these results, we can roughly extract the uniaxial anisotropy parameter $D \sim 0.4$ K (ref. 18). Below the crossover temperature, $T_c = 0.3$ K, identical magnetization curves indicate that QTM relaxation occurs from the ground state of the metastable well.

Assuming the typical giant-spin model, the spin hamiltonian describing an SMM is

$$\mathcal{H} = -DS_z^2 + E\left(S_x^2 - S_y^2\right) - \mu_B \mathbf{S}\cdot\hat{g}\cdot\mathbf{H}, \qquad (1)$$

where the first term represents the zero-field splitting, primarily resulting from spin–orbit coupling, and produces a uniaxial anisotropy barrier separating opposite projections of the spin along the axis of the wheel (magnetic easy axis). The second term is a second-order transverse anisotropy, which generates hard and medium axes in the plane of the wheel. The last term is the Zeeman energy resulting from the coupling of the spin with an externally applied magnetic field. For specific field values, known as QTM resonances ($H_k \approx kD/g\mu_B$, with $k = 0, 1, 2, \ldots$), levels on opposite sides of the barrier become degenerate. Off-diagonal hamiltonian terms break these degeneracies creating quantum superpositions that lead to tunnelling through the barrier and steps in the hysteresis loop. Using the extracted values of D (= 0.4 K) and S (= 7), we obtain QTM resonances at $H_0 = 0$, $H_1 = 0.29$ T and $H_2 = 0.58$ T, which coincide with three of the observed steps, more specifically, those labelled $k = 0$, $k = 1$(S) and $k = 2$ in Fig. 1d, where the derivatives of the magnetization curves for the same temperatures are presented for clarity. Significantly, however, the data also reveal extra resonances that are impossible to explain with this simple rigid-spin model. In Fig. 1d, three anomalous resonances are observed: one at $H = 0.45$ T present at low temperature (labelled $k = 1$(A)) and two that are only observed

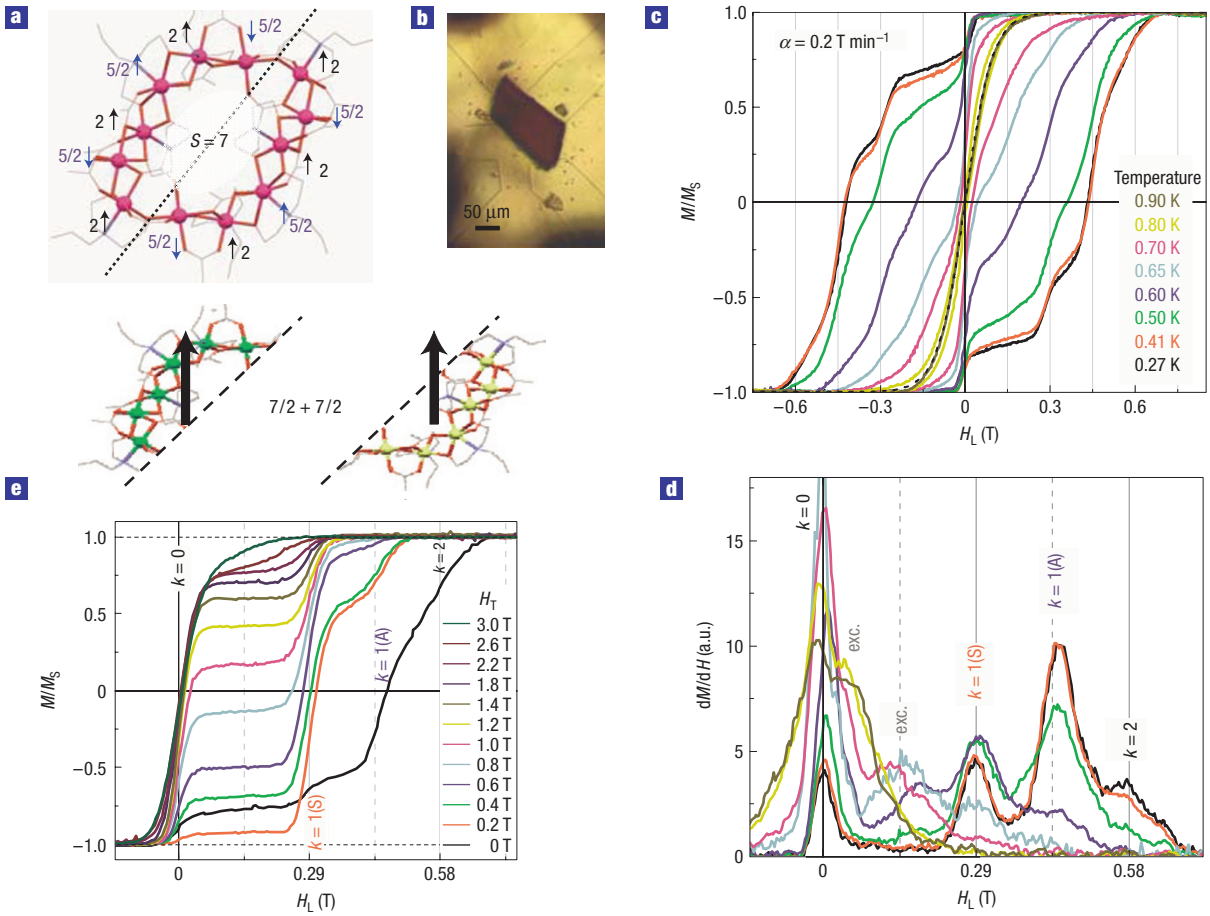

Figure 1 Structure and magnetism of the Mn_{12} wheel. a, Mn_{12} molecular wheel illustrating the exchange-coupled configuration of spins leading to a total spin $S = 7$ at low temperature. The dashed line separates the molecule into two weakly coupled halves of spin $S = 7/2$ each. **b**, Micrograph of the single-crystal sample placed on top of the cross-sensing area of a two-dimensional electron gas Hall-effect magnetometer. **c**, Hysteresis loops recorded at different temperatures with the field applied along the axis of the wheel (easy magnetic axis). The magnetization relaxation towards equilibrium is accelerated at the resonance fields (steps). **d**, Field derivative of data in **c**. The resonances are labelled according to the discussion in the text. **e**, Half-hysteresis loops (upright sweep) measured at $T = 270$ mK in the presence of a transverse field of different magnitudes.

for $T > 0.5$ K, at fields below 0.2 T (labelled exc.). As we will show below, these three resonances are key for the understanding of the studied system. Figure 1e shows the magnetization as a function of the longitudinal field, recorded in the presence of transverse fields of different magnitude applied along the hard magnetic axis in the plane of the wheel. Note that no QTM step appears between the resonances at $H = 0$ and $H = 0.29$ T, even for transverse fields as high as 3 T. Note also that this measurement was carried out at $T = 0.27$ K, and the resonances appearing in this field range (labelled exc.) are only present above 0.5 K.

To explain the data, we adopt a model in which the two halves of the wheel behave as ferromagnetically coupled units of spin $S_1 = S_2 = 7/2$ (see the Methods section). The hamiltonian describing this dimeric wheel is $\mathcal{H} = \mathcal{H}_1 + \mathcal{H}_2 + \mathcal{H}_{12}$, where $\mathcal{H}_1$ and $\mathcal{H}_2$ are the hamiltonians (from equation (1)) for the two halves, coupled by the Heisenberg superexchange interaction given by

$$\mathcal{H}_{12} = -J_z S_1^z S_2^z - J_\perp \left(S_1^x S_2^x + S_1^y S_2^y\right), \qquad (2)$$

where J_z and $J_\perp$ are positive (ferromagnetic) exchange constants characterizing the strength of the interaction. At the zeroth-order level of approximation, the eigenvectors of this hamiltonian can be written as products of the eigenvectors of each half of the molecule, $|S_1, m_1\rangle|S_2, m_2\rangle$ (or $|m_1, m_2\rangle$, to simplify the notation), where m_1 and m_2 are the projections of the spins of each half-wheel along the magnetic easy axis. The Heisenberg interaction couples the spin states of each half generating a new configuration of levels that can be grouped according to the projection, $M_S = m_1 + m_2$, of the total spin of the molecule onto the magnetic easy axis of the wheel. We illustrate this point in Fig. 2a by showing the lowest lying levels of the coupled system (with total spin projections $|M_S| = 6, 7$), which result from linear combinations of the states $|7/2, 7/2\rangle$, $|7/2, 5/2\rangle$ and $|5/2, 7/2\rangle$. The diagonal term of the Heisenberg interaction of equation (2) generates an exchange bias that shifts the energies of the levels by $J_z m_1 m_2$. For comparison, Fig. 2b shows the two lowest energy levels for a rigid-spin $S = 7$ for the entire molecule, whose dependence on the magnetic field has been calculated by exact diagonalization of the hamiltonian of equation (1) using $D = 0.405$ K, $E = 76$ mK and an isotropic $g = 2.0$. The levels intersect at the fields $H_R = k \times 0.29$ T (with $k = 0, 1, 2, \ldots$) yielding the QTM resonances $k = 0$, $k = 1$(S) and $k = 2$. However, owing to the fact that this description fails to account for all observed QTM resonances, this simple $S = 7$ model is deemed inadequate.

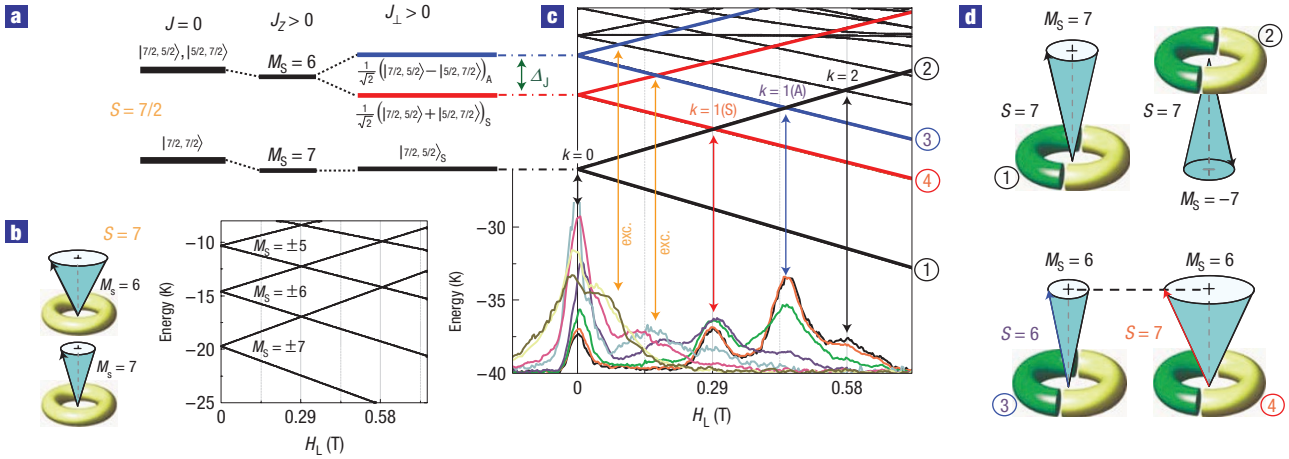

Figure 2 Energy of the exchange-coupled wheel halves. a, Lowest-lying energy levels of the total molecular spin resulting from exchange coupling of the spin, $S = 7/2$, of each half of the wheel. The Heisenberg interaction ($J_z > 0$) shifts the levels by a bias energy $J_z m_1 m_2$, whereas the transverse interaction (J_x, $J_y > 0$) breaks the degeneracy creating an exchange splitting between symmetric and antisymmetric states with easy-axis projection $M_S = 6$. **b**, Schematic diagrams and longitudinal field behaviour of the projection levels of the molecule assuming a rigid spin $S = 7$. **c**, Magnetic field behaviour of the levels assuming the exchange-coupled model of two spin-7/2 wheel halves. Data from Fig. 1d are included to clearly show the association between the measured QTM resonances and the crossing of the spin levels of the system. Orange lines indicate the level crossings contributing to the magnetic relaxation at high temperatures. **d**, Illustrations of the four levels involved in the QTM resonances observed at low temperature. Of special interest is the different spin length, $S = 6$, of state 3, which becomes quantum mechanically connected to state 2, with $S = 7$, at resonance $k = 1$(A); see text for details.

The second term of the interaction hamiltonian in equation (2) couples the two $S = 7/2$ spins and lifts the degeneracy between levels having the same M_S value, producing an exchange-splitting, Δ_J, between the symmetric and antisymmetric linear combinations of the unperturbed product states, see the example in Fig. 2a for the $M_S = 6$ states. As a consequence of this splitting, these two levels can be distinguished from each other by means of magnetic measurements in the presence of a longitudinal field, because they will produce an extra QTM resonance when they cross spin states of opposite spin projection (see below). Note that these levels have different total spin lengths, with the symmetric $S = 7$ and antisymmetric $S = 6$ states written as

$$|S=7, M_S=6\rangle = \frac{1}{\sqrt{2}}(|7/2,5/2\rangle + |5/2,7/2\rangle)_S$$
$$|S=6, M_S=6\rangle = \frac{1}{\sqrt{2}}(|7/2,5/2\rangle - |5/2,7/2\rangle)_A. \quad (3)$$

The magnetic field dependence of the lowest-lying levels of the coupled $S = 7/2$ half-wheels is shown in Fig. 2c. The results have been calculated by exact diagonalization of the total interaction hamiltonian using $D_{7/2} = 0.865\,\mathrm{K}(\sim 2D)$, $E_{7/2} = 0.156\,\mathrm{K}(\sim 2E)$ (where the subindex 7/2 relates to each wheel half), isotropic $g = 2.0$ and $J_z = J_\perp = 0.39\,\mathrm{K}$. This set of parameters closely reproduces each of the resonances observed in the experiment, including the thermally activated ones (labelled exc. in Figs 1d and 2c) observed above 0.5 K. Note that none of these resonances can be understood in terms of the rigid-spin model, as they involve levels that are split by the action of the exchange. The excellent agreement between the proposed model and all of the observed QTM resonances (low and high temperature) strengthens the validity of our description. To illustrate the proposed model, Fig. 2d contains representations of the four levels involved in the low-temperature resonances.

The dependence of the tunnel splitting on the transverse field, applied along the hard axis of the molecule, has been extracted for the resonances $k = 0$, $k = 1$(S) and $k = 1$(A) from an analysis of the height of the magnetization steps according to the Landau–Zener formula, which links the QTM probability (normalized ΔM) with the tunnel splitting, Δ. The results, shown in Fig. 3a, reveal oscillations in the probability corresponding to quantum interference between equivalent tunnelling trajectories, modulated with a period $\Delta H_T = 0.4\,\mathrm{T}$. We first focus on the symmetric resonances: the calculated splitting behaviours of the $k = 0$ and $k = 1$(S) resonances are shown in Fig. 3c (black and red lines, respectively). The solid lines are a result of exact diagonalization of the total interaction hamiltonian with the same parameters used in Fig. 2c and are in excellent agreement with the experiment. For comparison, the dotted lines are calculated from the hamiltonian of equation (1) for a rigid spin $S = 7$ with the parameters used in Fig. 2b, illustrating the similarity between both descriptions as relating to the crossing of symmetric states.

The primary focus of this work is to shed light on the origin of resonance $k = 1$(A), which results from the avoided level crossing of the symmetric $|S = 7, M_S = -7\rangle$ and antisymmetric $|S = 6, M_S = 6\rangle$ states, labelled 2 and 3 in Fig. 2d, respectively. Given that the other resonances could be well explained with a rigid-spin model, this is the only resonance observed in the low-temperature magnetization that requires the exchange-coupled dimer description. One interesting aspect of our results is the fact that the symmetric and antisymmetric nature of the levels involved in this resonance requires further interaction terms in the hamiltonian, which are capable of breaking the degeneracy and producing a tunnel splitting of adequate magnitude to explain the observed QTM rate. Indeed, this is an old question within the SMM community, because QTM is commonly observed in most SMMs at forbidden resonances, even when the required interactions are either absent or clearly insufficient to explain the experimental results[17]. Two possible sources of broken degeneracy, appropriate

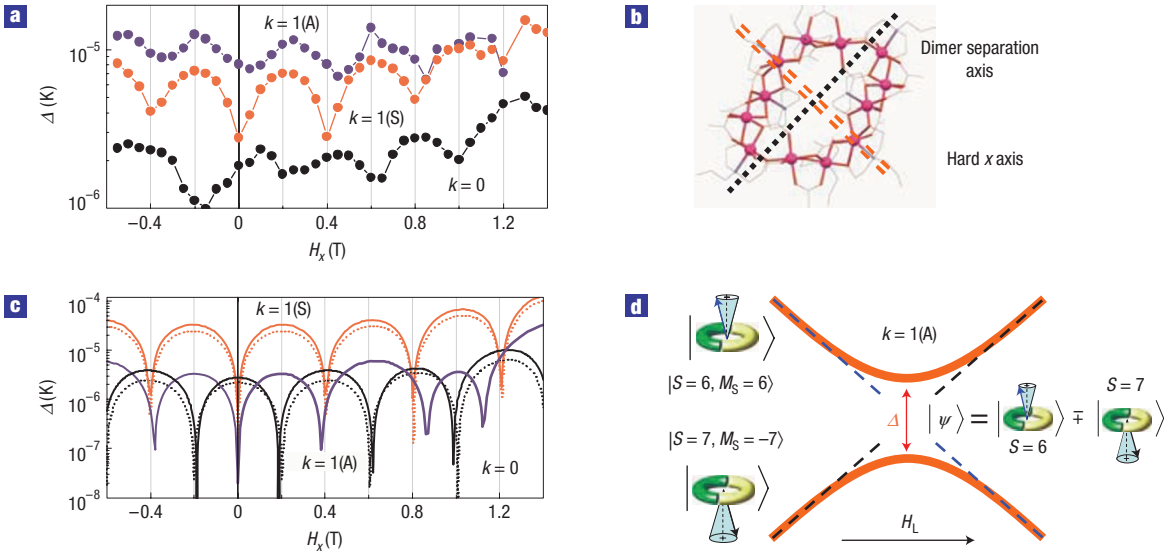

Figure 3 Quantum interference effects on the tunnel splittings. a, Behaviour of the tunnel splittings, Δ_k, of resonances $k=0$, $k=1$(S) and $k=1$(A) as a function of a transverse magnetic field applied along the hard anisotropy (x) axis in the plane of the wheel. The splittings of all resonances vanish at certain field values that are regularly spaced by a period of 0.4 T. These oscillations correspond to destructive quantum interference of opposite QTM trajectories. The phase shift between resonances $k=0$ and $k=1$(S) is a consequence of the spin parity effect, which breaks the zero-field degeneracy of the ground state of an integer spin ($\Delta_{k=0}>0$ at $H=0$). Resonance $k=1$(A) also shows the same oscillation period, with a small field shift of $\sim$0.05 T with respect to resonance $k=1$(S). **b**, Illustration of the direction of the hard anisotropy axis in the plane of the molecule (almost perpendicular to the axis separating the two wheel halves). **c**, Calculated transverse field dependence of the tunnel splittings of resonances $k=0$, $k=1$(S) using the same parameters as in Fig. 2c plus a Dzyaloshinskii–Moriya interaction for resonance $k=1$(A). **d**, Representation of the avoided crossing of levels at resonance $k=1$(A). The tunnel splitting, Δ, separates the symmetric and antisymmetric superposition states with different spin length.

to the symmetry and chemical composition of the system are discussed in the Methods section.

Of most relevance is the fact that this resonance connects two magnetic states of different spin length. Figure 3d exemplifies this field dependence in the vicinity of the resonance, where the symmetric and antisymmetric superposition states of different spin length,

$$|\psi\rangle = \frac{1}{\sqrt{2}}\left(|S=6, M_S=6\rangle \pm |S=7, M_S=-7\rangle\right),$$

are separated by the tunnel splitting, Δ.

Quantum superpositions of states with different spin length have recently been observed in the paramagnetic heterometallic Cr_7Ni wheel by means of neutron scattering experiments[19]. However, this is the first time that a uniaxial SMM has shown this effect. Until now, only transverse oscillations involving a fixed-length (rigid) spin between opposite M_S projections have been reported for SMMs (ref. 15). The significance of our result resides in the fact that a transverse field can be used to modulate the tunnel splitting, which constitutes firm evidence for quantum interference associated with the total spin length of an exchange-coupled dimer of molecular nanomagnets.

QTM and quantum coherence in antiferromagnetic and ferrimagnetic exchange-coupled molecular clusters has been, and continues to be a topic of intense theoretical study[20,21]. Of particular relevance to our work is the topological quenching of the tunnel splittings in SMMs that was predicted by Loss *et al.*[22] and von Delft and Henley[23] for semi-integer spins with Kramers' degeneracies. Garg[24] extended this result for integer spins with quadratic anisotropy, and Leuenberger and Loss[25] generalized it for integer spins for a general class of magnetic anisotropy. Berry-phase interference has been experimentally observed in the Fe_8 (ref. 15) and Mn_{12} (refs 16,17) SMMs. Nevertheless, topological effects on the QTM involving exchange-coupled SMMs have not been studied theoretically. However, the development of geometrical phases in systems of two entangled spin-1/2 particles precessing in a time-independent uniform magnetic field has been theoretically considered by Sjoqvist[26]. This author showed that when there is an exchange interaction between the particles, the geometrical phase acquired by the system during precession cannot be reduced to the sum of the phases of each independent particle (which is the case when the interaction is absent). This work provides a clear demonstration of the importance of the entanglement for the geometric phase of quantum systems with interacting parts, which is particularly relevant in two-photon interferometry studies. Note that the QTM for non-interacting SMMs can be described in terms of a spin precessing in imaginary time around an effective uniform magnetic field, where topological interference between opposite tunnel trajectories with different geometrical phases leads to quenching of the tunnelling splitting[15–17,22–25]. In a similar way, it could be speculated that in the case of two interacting SMMs, as is the case for the system studied here, the observed oscillation of the tunnelling probability may be attributed to topological interference (two competing Berry phases). Although a formal theoretical background is absent in the case of pairs of exchange-interacting SMMs and, therefore, this interpretation is speculative, the results provided here constitute a remarkably clean example of an exchange-coupled pair of quantum tunnelling giant spins, providing a solid experimental basis for any future theoretical studies of topological effects in interacting systems.

METHODS

CHEMICAL AND PHYSICAL DESCRIPTION OF THE SAMPLE

The Mn_{12}-based wheel $[Mn_{12}(Adea)_8(CH_3COO)_{14}]\cdot 7CH_3CN$ was synthesized using the ligand *n*-allyl-2,2′-iminodiethanol. This single-stranded wheel is a

structural analogue of a previously reported series of Mn_{12} wheels[27,28] and consists of six Mn(II) ($S = 5/2$) and six Mn(III) ($S = 2$) ions alternating in a ring-shaped topology with eight *n*-allyl-2,2′-iminodiethanol dianions. Addition of one equivalent of the ligand *n*-allyl-2,2′-iminodiethanol to Mn(II) acetate in dichloromethane gives a red coloured solution. After a further addition of one equivalent of triethylamine, the solution turns a deep reddish brown and is allowed to stir overnight. A white precipitate is obtained which is filtered off. A subsequent evaporation of the filtrate by vacuum distillation yields oil, to which 100 ml of acetonitrile is added. Slow evaporation of the acetonitrile solution leads to the formation of plate-shaped crystals after approximately one week. The crystal structure indicates that four Mn(II) ions and six Mn(III) ions are six-coordinate, with the remaining two Mn(II) ions being seven-coordinate with a pentagonal-bipyramidal coordination geometry. This complex crystallizes in the P-1 space group with seven acetonitrile solvent molecules per wheel and one Mn_{12} wheel molecule in the unit cell.

Exchange interactions between neighbouring manganese ions in the wheel lead to the spin configuration shown in Fig. 1a, which represents the molecule in its $S = 7$ ground state. Estimates for the strengths of the exchange interactions carried out for a similar compound[29] reveal that the exchange interaction between two manganese pairs at opposite sides of the wheel is over two orders of magnitude weaker than that of the other pairs of the wheel, splitting the molecule into two half-wheels of spin $S = 7/2$ each, which can be modelled as ferromagnetically coupled units giving rise to a total $S = 7$ ground state.

HYPERFINE AND SYMMETRY HAMILTONIAN TERMS OF THE MOLECULE

Further terms in the hamiltonian of equation (1) arising from the composition and symmetry lowering of the molecule can break the degeneracy of resonance $k = 1$(A) and explain the observed tunnelling relaxation rates. One potential source of broken degeneracy involves hyperfine interactions, because they can mix spin states making the transition moment integrals non-zero[30]. However, the mixing in this case is only of the order of $\sim A^2/J^2$, where A ($\ll J$) is the hyperfine interaction constant. Our estimates indicate that this interaction is clearly insufficient to explain the observed tunnel splitting values in resonance $k = 1$(A). Aside from mixing, the degeneracy between the two levels at resonance $k = 1$(A) can only be broken by an antisymmetric coupling, such as the Dzyaloshinskii–Moriya exchange interaction resulting from spin–orbit coupling. However, X-ray diffraction data reveal an inversion centre of symmetry that prevents a Dzyaloshinskii–Moriya interaction in this molecule. It is possible that slight deformations at low temperature distort the symmetry of the molecule allowing Dzyaloshinskii–Moriya coupling, although we do not have clear evidence to support this hypothesis, which will be the focus of future investigation. For illustrative purposes, we have solved the complete interaction hamiltonian including a spin–orbit correction using the model given in ref. 31 in which a Dzyaloshinskii–Moriya term, $-J\sin\phi(S_1^xS_2^y - S_1^yS_2^x)$, is added to the hamiltonian in equation (2), where J_z and $J_\perp$ are substituted by J and $J\cos\phi$, respectively. In this description, ϕ represents the angle of precession of the electron spin hopping between the two Mn ions of the pairs separating the wheel halves through the oxygen bridge. The calculated data shown in Fig. 3c were obtained with $J = 0.390$ K and $\phi = 1.5°$. As can be seen in Fig. 3c, this calculation is in good qualitative agreement with the experimental behaviour, accounting both for the magnitude of the tunnel splitting and the observed interference pattern parity (positions of the interference minima).

MAGNETIC MEASUREMENTS

The experiments were carried out on a $20 \times 50 \times 100\,\mu m^3$ single crystal placed on top of a high-sensitivity micro-Hall-effect magnetometer as shown in Fig. 1b. Magnetization hysteresis loops were recorded by applying a magnetic field along the easy magnetic axis, which coincides with the axis of the wheel, at different temperatures down to 0.27 K in an Oxford Instruments ^{3}He cryostat.

Received 18 October 2007; accepted 24 January 2008; published 2 March 2008.

References

1. Loss, D. & DiVincenzo, D. P. Quantum computation with quantum dots. *Phys. Rev. A* **57**, 120–126 (1998).
2. Leuenberger, M. & Loss, D. Quantum computing in molecular magnets. *Nature* **410**, 789–793 (2001).
3. Wernsdorfer, W., Aliaga-Alcade, N., Hendrickson, D. N. & Christou, G. Exchange-biased quantum tunneling in a supramolecular dimer of single-molecule magnets. *Nature* **416**, 406–409 (2002).
4. Hill, S., Edwards, R. S., Aliaga-Alcade, N. & Christou, G. Quantum coherence in an exchange-coupled dimer of single-molecule magnets. *Science* **302**, 1015–1018 (2003).
5. Prokof'ev, N. V. & Stamp, P. C. E. Theory of the spin bath. *Rep. Prog. Phys.* **63**, 669–726 (2000).
6. Chudnovsky, E. M. Universal decoherence in solids. *Phys. Rev. Lett.* **92**, 120405 (2004).
7. del Barco, E., Kent, A. D., Yang, E. C. & Hendrickson, D. N. Quantum superposition of high spin states in the single molecule magnet Ni_4. *Phys. Rev. Lett.* **93**, 157202 (2004).
8. Wernsdorfer, W., Mailly, D., Timco, G. A. & Winpenny, R. E. P. Resonant photon absorption and hole burning in Cr_7Ni antiferromagnetic rings. *Phys. Rev. B* **72**, 060409 (2005).
9. Waldmann, O., Dobe, C., Mutka, H., Furrer, A. & Güdel, H. U. Neel-vector tunneling in antiferromagnetic molecular clusters. *Phys. Rev. Lett.* **95**, 057202 (2005).
10. Bal, M. *et al.* Non-equilibrium magnetization dynamics in the Fe_8 single-molecule magnet induced by high-intensity microwave radiation. *Europhys. Lett.* **71**, 110–116 (2005).
11. Ardavan, A. *et al.* Will spin-relaxation times in molecular magnets permit quantum information processing? *Phys. Rev. Lett.* **98**, 057201 (2007).
12. Friedman, J. R., Sarachik, M. P., Tejada, J. & Ziolo, R. Macroscopic measurements of resonant magnetization tunneling in high-spin molecules. *Phys. Rev. Lett.* **76**, 3830–3833 (1996).
13. Thomas, L. *et al.* Macroscopic quantum tunneling of magnetization in a single crystal of nanomagnets. *Nature* **383**, 145–147 (1996).
14. Bokacheva, L., Kent, A. D. & Walters, M. A. Crossover between thermally assisted and pure quantum tunneling in molecular magnet Mn_{12}-acetate. *Phys. Rev. Lett.* **85**, 4803–4806 (2000).
15. Wernsdorfer, W. & Sessoli, R. Quantum phase interference and parity effects in magnetic molecular clusters. *Science* **284**, 133–135 (1999).
16. del Barco, E., Kent, A. D., Rumberger, E. M., Hendrickson, D. N. & Christou, G. Symmetry of magnetic quantum tunneling in single molecule magnet Mn_{12}-acetate. *Phys. Rev. Lett.* **91**, 047203 (2003).
17. del Barco, E. *et al.* Magnetic quantum tunneling in the single-molecule magnet Mn_{12}-acetate. *J. Low. Temp. Phys.* **140**, 119–174 (2005).
18. Chudnovsky, E. M. & Tejada, J. *Quantum Tunneling of the Magnetization* (Oxford Univ. Press, New York, 1983).
19. Carretta, S. *et al.* Quantum oscillations of the total spin in a heterometallic antiferromagnetic ring: Evidence from neutron spectroscopy. *Phys. Rev. Lett.* **98**, 167401 (2007).
20. Chiolero, A. & Loss, D. Macroscopic quantum coherence in ferrimagnets. *Phys. Rev. B* **56**, 738–746 (1997).
21. Meier, F. & Loss, D. Electron and nuclear spin dynamics in antiferromagnetic molecular rings. *Phys. Rev. Lett.* **86**, 5373–5376 (2001).
22. Loss, D., DiVincenzo, D. P. & Grinstein, G. Suppression of tunneling by interference in half-integer-spin particles. *Phys. Rev. Lett.* **69**, 3232–3235 (1992).
23. von Delft, J. & Henley, C. L. Destructive quantum interference in spin tunneling problems. *Phys. Rev. Lett.* **69**, 3236–3239 (1992).
24. Garg, A. Topologically quenched tunnel splitting in spin systems without Kramers' degeneracy. *Europhys. Lett.* **22**, 205–210 (1993).
25. Leuenberger, M. N. & Loss, D. Spin tunneling and topological selection rules for integer spins. *Phys. Rev. B* **63**, 054414 (2001).
26. Sjöqvist, E. Geometric phase for entangled spin pairs. *Phys. Rev. A* **62**, 022109 (2000).
27. Rumberger, E., Zakharov, L., Rheingold, A. & Hendrickson, D. N. Synthesis and magnetic properties of wheel shaped $[Mn_{12}]$ and $[Fe_8]$ complexes. *Inorg. Chem.* **43**, 6531–6533 (2004).
28. Rumberger, E. *et al.* Wheel shaped $[Mn_{12}]$ single molecule magnets. *Inorg. Chem.* **44**, 2742–2752 (2005).
29. Foguet-Albiol, D. *et al.* DFT computational rationalization of an unusual spin ground state in an Mn-12 single-molecule magnet with a low-symmetry loop structure. *Angew. Chem. Int. Edn* **44**, 897–901 (2005).
30. Dugan, D. M. & Hendrickson, D. N. Magnetic exchange interactions in transition-metal dimers 3: Nickel (II) di-μ-cyanato, di-μ-thiocyanato, and di-μ-selenocyanato complexes and related outer-sphere copper (II) complexes. *Inorg. Chem.* **13**, 2929–2940 (1974).
31. Bonesteel, N. E. Theory of anisotropic superexchange in insulating cuprates. *Phys. Rev. B* **47**, 11302–11313 (1993).

Acknowledgements

We gratefully acknowledge fruitful discussions with Eduardo Mucciolo and Michael Leuenberger. E.d.B., S.H. and D.N.H. acknowledge support from the US National Science Foundation (DMR0706183 and DMR0747587), (DMR0506946 and DMR0239481) and (CHE0350615), respectively. Correspondence and requests for materials should be addressed to E.d.B.

Author contributions

C.M.R. and E.d.B. planned and carried out the experiments. S.H. helped in the interpretation of the results. S.J.S., C.C.B. and D.N.H. synthesized the compound. All authors discussed the results and contributed to their interpretation.